Determination of Ligand-Field Parameters and f-Electronic Structures of Hetero-Dinuclear Phthalocyanine Complexes with a Diamagnetic Yttrium(III) and a Paramagnetic Trivalent Lanthanide Ion

Naoto Ishikawa,*,† Tomochika Iino, and Youkoh Kaizu*

Department of Chemistry, Tokyo Institute of Technology, O-okayama, Meguro-ku, Tokyo 152-8551, Japan

Received: April 8, 2002; In Final Form: August 14, 2002

Ligand-field parameters of the f-electronic systems in a series of dinuclear lanthanide phthalocyaninato complexes have been determined. To study the systems without intermetallic interactions, new asymmetric hetero-dinuclear lanthanide phthalocyaninato complexes, PcYPcLnPc* (Pc = dianion of phthalocyanine, Pc* = dianion of 2,3,9,10,16,17,23,24-octabutoxyphthalocyanine and Ln = Tb, Dy, Ho, Er, Tm, and Yb), were prepared. The synthesis of the dinuclear complexes were achieved by the reaction of Pc_2Y, H_2Pc*, and Ln(acac)$_3$·n(H_2O). Measurements of magnetic susceptibility of powder samples of PcYPcLnPc* were carried out over the temperature range from 1.8 to 303 K. Using the multidimensional simplex minimization method, we obtained a set of ligand-field parameters that reproduces both the ^{1}H NMR paramagnetic shifts and the magnetic susceptibility data. Ligand-field-splitting structure of the ground-state multiplets of the six lanthanide systems has been elucidated. A new computational approach to obtain ligand-field parameters is proposed for the situations in which sharp emission or absorption bands or both are not available.

Introduction

Phthalocyanines and porphyrins have been known to form so-called "triple-decker" complexes composed of three planar ligands and two lanthanide ions.[1−3] In dinuclear complexes with cerium(III), the ionic radius of which is the largest in the lanthanide series, the Ce−Ce distance has been reported to be 3.752 Å for $Ce_2(OEP)_3$,[3] 3.84 Å for (TPP)Ce(Pc(OMe)$_8$)Ce(TPP), and 3.66 Å for (Pc)Ce(T(*p*-MeOP)P)Ce(Pc).[4,5] The metal-to-metal distances in dinuclear complexes with other lanthanide ion pairs are expected to be shorter than the dicerium complexes because of the lanthanide contraction. With these distances, it is likely that there are sizable interactions between the two f-electronic systems. Despite the fact that this particularly interesting and unique feature has been known for years, there are no decisive studies elucidating the interaction between the two f systems. In fact, even electronic structures of the f systems in mononuclear double-decker complexes have not been well understood yet.

Theoretical investigations on the electronic structure of the triple-decker complexes have been so far mainly focused on the π systems of the ligands. For phthalocyanine triple-decker systems, the authors have reported studies on the electronic spectrum in the UV region.[6,7] The spectral changes from monomeric complexes were explained by the interactions involving only π electrons, that is, exciton coupling and charge resonance.[8] The characteristic bands in the near-IR region caused by one- or two-electron oxidation[9,10] were also explained with the interaction terms among the three highest occupied π orbitals on the three ligands.[11] The only difference in lanthanide ions that had to be considered was the change in the ionic radius, which varies the geometric structure of the complexes and thereby the interaction terms between π orbitals belonging to different ligands.

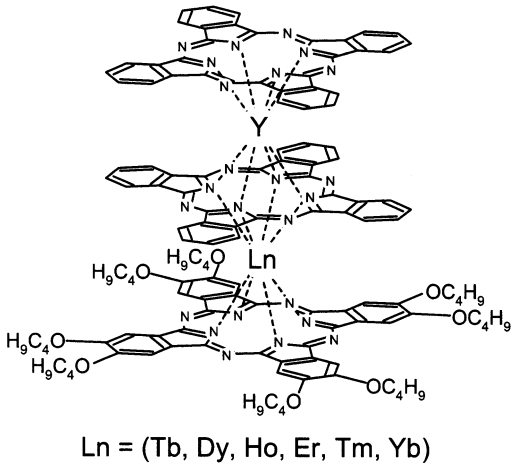

Figure 1. Schematic diagram of PcYPcLnPc(OC$_4$H$_9$)$_8$.

To study the magnetic properties of the dinuclear complexes, we need to examine explicitly the f-electronic systems. It is naturally anticipated that the magnetic properties of the dinuclear complexes are determined by two terms, the ligand field for each f system and the interaction between the two f systems. The interaction term is, of course, only possible to be studied after knowing the ligand-field terms.

The purpose of the present paper is to determine the ligand-field term of the dinuclear lanthanide complexes. To investigate the ligand-field terms alone, one first needs the systems that contain only one paramagnetic lanthanide ion. To this end, we have prepared a series of new hetero-dinuclear Pc complexes, PcYPcLnPc* (Figure 1, Pc* = dianion of 2,3,9,10,16,17,23,24-octabutoxyphthalocyanine and Ln = Tb, Dy, Ho, Er, Tm, and Yb). In what follows, the notation "[Y, Ln]" will be used to refer to PcYPcLnPc*. We employed a synthetic route similar to the "monomer + dimer" method reported by Lindsey et al. for (TTP)Ce(tBPc)Eu(tBPc).[12,13] Through measurements and

* To whom correspondence should be addressed.
† E-mail: ishikawa@chem.titech.ac.jp.

10.1021/jp0209244 CCC: $22.00
Published on Web 09/19/2002

theoretical analysis of magnetic susceptibility and ^{1}H NMR of the complexes, we have determined the LF (ligand-field) parameters that describe the f-electronic structures of the [Y, Ln] series, as shown below.

The past studies on the multiplet structures of lanthanide f systems were reported only for the cases for which sharp emission or absorption bands or both are available. In general, it is difficult to obtain LF parameters unless information about the energies of the multiplet sublevels is provided as in the above cases. In the present case, however, neither fluorescence nor absorption spectra associated with lanthanide centers are obtainable because of the low-lying Pc-centered energy levels quenching the lanthanide fluorescence and the extremely intense Pc-centered absorption bands concealing the lanthanide-centered bands. One must, therefore, develop a method to determine the LF parameters using the experimental data that does not provide direct information about the multiplet structure. In the present paper, we present a new approach to obtain LF parameters from paramagnetic shift in ^{1}H NMR and temperature dependence of magnetic susceptibility.

Experimental Section

General Procedure for the Synthesis of PcYPcLnPc* (Ln = Tb, Dy, Ho, Er, Tm, Yb, and Y). Twenty milligrams of Pc_2Y, 20 mg of H_2Pc*, 80 mg of $Ln(acac)_3 \cdot n(H_2O)$ (Ln = Tb, Dy, Ho, Er, Tm, Yb, or Y), and 5 mL of 1,2,4-triclorobenzene were put in a 10 mL round flask equipped with a condenser. The mixture was heated on an oil bath set at 60 °C with mechanical stirring until the entire solid was dissolved. Then the bath temperature was increased, and the mixture continued refluxing for 3 h with careful monitoring by UV spectrum. The reaction solution was cooled to room temperature, and 80 mL of methanol was added. The precipitant was filtered, washed with methanol, and extracted with dichloromethane. The extract solution was chromatographed on a silica gel column (Silica Gel 60, Kanto Chemicals, particle size 40−60 μm). Using dichloromethane as an eluent, we eluted a green band of unreacted Pc_2Y initially. The second blue-green band of the aimed substance was collected. The solution was concentrated, methanol was added, and the solution was filtered. The chromatographic separation was repeated until the band of unreacted Pc_2Ln disappeared. The final product PcLnPcYPc* was obtained as a blue-black powder (typically 25 mg). The powder was recrystallized from CH_2Cl_2/hexane. The compounds were identified by elemental analysis and ^{1}H NMR spectrum. Anal. Calcd for $C_{128}H_{112}N_{24}O_8TbY$ ([Y, Tb]): C, 65.08; H, 4.78; N, 14.23. Found: C, 64.92; H, 4.83; N, 14.06. Anal. Calcd for $C_{128}H_{112}N_{24}O_8DyY$ ([Y, Dy]): C, 64.98; H, 4.77; N, 14.21. Found: C, 64.81; H, 4.85; N, 13.91. Anal. Calcd for $C_{128}H_{112}N_{24}O_8HoY$ ([Y, Ho]): C, 64.91; H, 4.76; N, 14.19. Found: C, 64.95; H, 4.98; N, 14.14. Anal. Calcd for $C_{128}H_{112}N_{24}O_8ErY$ ([Y, Er]): C, 64.85; H, 4.76; N, 14.18. Found: C, 64.58; H, 4.87; N, 14.04. Anal. Calcd for $C_{128}H_{112}N_{24}O_8TmY$ ([Y, Tm]): C, 64.80; H, 4.75; N, 14.17. Found: C, 64.99; H, 4.45; N, 13.91. Anal. Calcd for $C_{128}H_{112}N_{24}O_8YbY$ ([Y, Yb]): C, 64.69; H, 4.75; N, 14.14. Found: C, 64.57; H, 4.85; N, 14.28. Anal. Calcd for $C_{128}H_{112}N_{24}O_8Y_2$ ([Y, Y]): C, 67.07; H, 4.92; N, 14.67. Found: C, 66.79; H, 5.01; N, 14.40.

Through the NMR measurements, we have confirmed that there was no contamination by [Ln, Ln] or [Ln, Y] complexes in all cases examined. This indicates that there was no cleavage of Pc_2Y during the formation of [Y, Ln], unlike the reaction of $PcLi_2$, $Ln(acac)_3$, and $Ln(Pc(OC_8H_{17})_8)_2$, which produced a mixture of $(Pc)Ln(Pc(OC_8H_{17})_8)Ln(Pc(OC_8H_{17})_8)$ and $(Pc)Ln(Pc(OC_8H_{17})_8)Ln(Pc)$.[14]

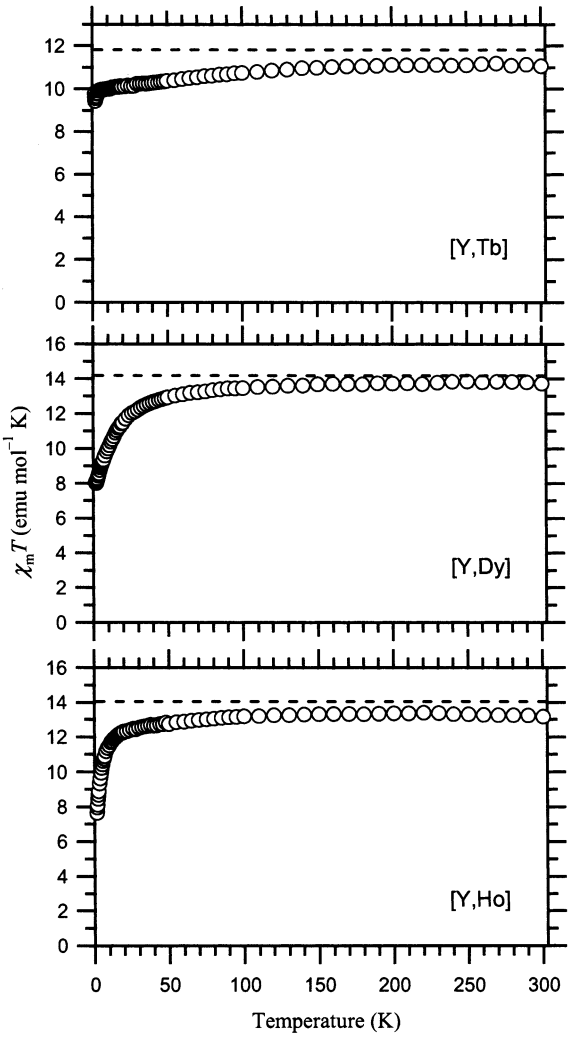

Figure 2. Plots of $\chi_m T$ versus temperature, T, for [Y, Tb] (top), [Y, Dy] (center), and [Y, Ho] (bottom).

Measurements. Magnetic susceptibility measurements were carried out on a Quantum Design MPMS-5 SQUID (superconducting quantum interference device) magnetometer. As the correction from the diamagnetic susceptibility contribution in each the sample, corresponding experimental data for PcYPcYPc* was used. ^{1}H NMR spectra of the complexes were measured in $CDCl_3$ solution at 30 °C on a JEOL Lambda-300 NMR spectrometer.

Results and Discussion

SQUID Measurements. The plots in Figure 2 show temperature dependence of $\chi_m T$ values (molar magnetic susceptibility, χ_m, times temperature, T) of [Y, Tb], [Y, Dy], and [Y, Ho]. In the room-temperature range, $\chi_m T$ approaches the corresponding value of a free trivalent ion in each case: $\chi_m T$ = 11.81 emu K/mol for Tb^{3+}, 14.18 emu K/mol for Dy^{3+}, 14.07 emu K/mol for Ho^{3+}. The $\chi_m T$ value of [Y, Tb] gradually decreases with lowering temperature and reaches 9.58 emu K/mol at 2.0 K. The [Y, Dy] case shows a greater degree of reduction in $\chi_m T$. The value falls to 8.07 emu K/mol at 2 K. [Y, Ho] shows a similar tendency: $\chi_m T$ at 2 K is 7.93 emu K/mol. The curvatures in the latter two cases show clear differences in the range 100−1.8 K.

TABLE 1: Assignments of ^{1}H NMR Signals, δ, and Paramagnetic Shift, $\Delta\delta$, of PcYPcLnPc$(OC_4H_9)_8$

	Ln	$\alpha(Pc^O)^a$	$\beta(Pc^O)^a$	$\alpha(Pc^C)^a$	$\beta(Pc^C)^a$	α(Pc*)	OCH_2(1)	OCH_2(2)
δ (ppm)	Y	8.46	8.06	8.99	8.73	7.95	4.72	4.44
	Tb	24.08	9.77	−65.39	−31.67	−66.69	−30.33	−20.85
	Dy	16.40	8.96	−27.83	−10.94	−29.81	−12.88	−8.19
	Ho	11.31	8.37	−4.27	1.81	−5.78	−1.61	−0.17
	Er	4.99	7.64	25.12	17.81	24.52	12.54	10.16
	Tm	3.77	7.56	31.00	20.91	31.00	15.61	12.35
	Yb	7.83	7.94	11.40	10.09	10.68	6.02	5.38
$\Delta\delta$ (ppm)	Tb	15.62	1.71	−74.38	−40.40	−74.64	−35.05	−25.29
	Dy	7.94	0.90	−36.82	−19.67	−37.76	−17.60	−12.63
	Ho	2.85	0.31	−13.26	−6.92	−13.73	−6.33	−4.61
	Er	−3.47	−0.42	16.13	9.08	16.57	7.82	5.72
	Tm	−4.69	−0.50	22.01	12.18	23.05	10.89	7.91
	Yb	−0.63	−0.12	2.41	1.36	2.73	1.30	0.94
$\Delta\delta/\Delta\delta(\alpha(Pc^C))$	Tb	−0.21	−0.02	1.00	0.54	1.00	0.47	0.34
	Dy	−0.22	−0.02	1.00	0.53	1.03	0.48	0.34
	Ho	−0.21	−0.02	1.00	0.52	1.04	0.48	0.35
	Er	−0.22	−0.03	1.00	0.56	1.03	0.48	0.35
	Tm	−0.21	−0.02	1.00	0.55	1.05	0.49	0.36
	Yb	−0.26	−0.05	1.00	0.56	1.13	0.54	0.39

[a] Pc^O and Pc^C denote Pc on the outer side and that on the center, respectively.

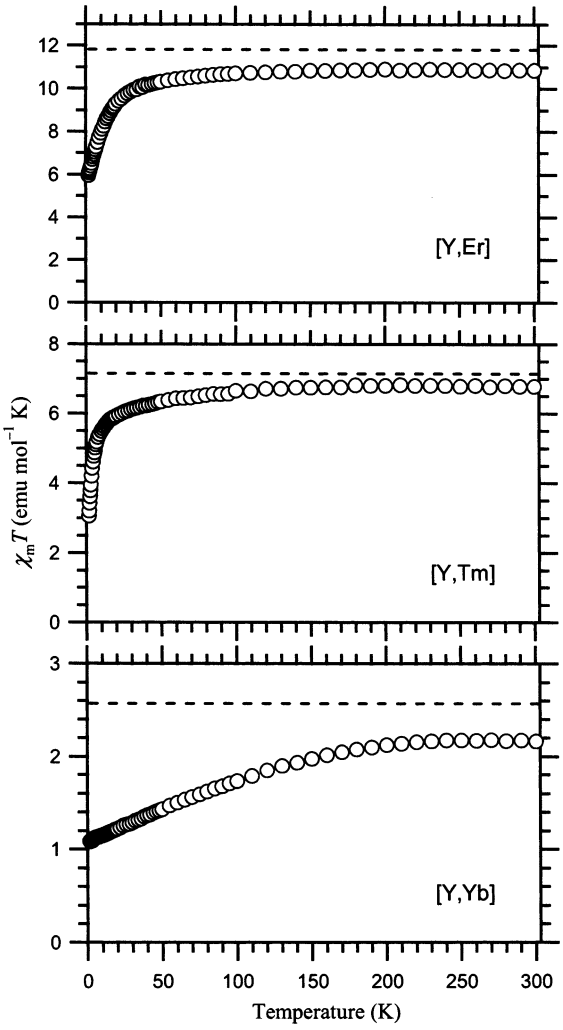

Figure 3. Plots of $\chi_m T$ versus temperature T for [Y, Er] (top), [Y, Tm] (center), and [Y, Yb] (bottom).

The plots of $\chi_m T$ vs T of [Y, Er], [Y, Tm], and [Y, Yb] are shown in Figure 3. Again, the curves approach the $\chi_m T$ value of a free Dy^{3+} (11.81 emu K/mol), Tm^{3+} (7.15 emu K/mol) and Yb^{3+} (2.57 emu K/mol), respectively, at room temperature. Lowering temperature decreases $\chi_m T$ in the three cases in different manners. The $\chi_m T$ values at 2 K are 5.96 emu K/mol in [Y, Er], 3.20 emu K/mol in [Y, Tm], and 1.08 emu K/mol [Y, Yb].

^{1}H NMR Measurements. Table 1 shows results of the measurements of ^{1}H NMR spectra of [Y, Ln] complexes. The signals of the protons on the Pc rings in the diamagnetic [Y, Y] are observed in the region from ca. 8 to 9 ppm. A COSY measurement showed that the signals at 8.99 and 8.73 ppm belong to the same Pc ligand and those at 8.46 and 8.06 ppm to another Pc. Arnold et al. have shown by comparing data for (Pc)Y(Pc**)Y(Pc**) and (Pc)Y(Pc**)Y(Pc) (Pc** = Pc-$(OC_8H_{17})_8$) that an α proton is observed at higher frequency than the β proton in the same Pc and that a proton on the center Pc is at higher frequency than the corresponding proton on the outer Pc.[15] According to this, the signals at 8.99 and 8.73 ppm are assigned to α and β protons on the center Pc, and those at 8.46 and 8.06 ppm are assigned to α and β on the outer Pc, respectively. The signal at 7.95 ppm is assigned to the α proton of Pc*. The protons of the methylene next to the oxygen atoms are observed at 4.72 and 4.44 ppm corresponding to the two nonequivalent positions in [Y, Y].

In the other [Y, Ln] systems, paramagnetic shifts in the signals are observed. In the present case, in which all of the protons are separated from the lanthanide ions by four atoms at least, Fermi contact contribution to the paramagnetic shift is expected to be far smaller than the magnetic dipolar contribution. The latter contribution is proportional to a geometric factor, $(1 - 3\cos^3\theta)/R^3$, where R is the distance between the paramagnetic center and the proton under consideration and θ is the azimuth of the proton with respect to the quantization axis, that is, the C_4 axis. Using geometric parameters R and θ of Pc_3Y_2 obtained by a density functional theory calculation, we carried out the assignments of the signals.

The molecular geometry optimization of Pc_3Y_2 was performed with B3LYP theory[16] on the Gaussian 98[17] program. The basis set employed was LANL2DZ, in which Los Alamos effective core potential plus double-ζ function[18] is used for Y atom and Dunning/Huzinaga full double-ζ function[19] for H, C, and N atoms. The result is listed in Table 2. Because of the large molecular size, use of basis sets with polarization functions was not feasible. Due to the lack of polarization functions on Pc, the prediction on the distortion from planarity in the Pc

TABLE 2: Geometric Factor $(1 - 3\cos^3\theta)/R^3$ and the Distance between Two Y Atoms r(Y−Y) in D_{4h} Pc_3Y_2 Obtained by a DFT Calculation (LANL2DZ/B3LYP)[a]

	α(Pc[1])[a]	β(Pc[1])[b]	α(Pc[2])[b]	β(Pc[2])[b]	α(Pc[3])[b]	β(Pc[3])[b]	r(Y−Y), Å
$10^3(1 - 3\cos^3\theta)/R^3$	−0.836	−0.255	3.137	1.740	2.582	1.267	3.571
relative values	−0.267	−0.081	1.000	0.555	0.823		

[a] Origin of the coordinates is on the Y atom between Pc[2] and Pc[3]. [b] Pc[1] and Pc[3] denote Pc on the outer side. Pc[2] is in the center.

ligand is not fully reliable. One must, therefore, be cautious about the geometric parameter in the outer Pc rings. On the contrary, the parameter for the central Pc, which is planar, is much more reliable.

Table 1 shows the paramagnetic shifts, $\Delta\delta$, which are defined as (chemical shift for a proton in [Y, Ln]) − (that of the corresponding proton in [Y, Y]). The largest paramagnetic shift is observed in the α protons on the center Pc and Pc* in all the six cases. [Y, Tb] shows the largest shift in each proton case. The magnitude of the shift is reduced in [Y, Dy] and [Y, Ho], and then the direction of the shift changes in [Y, Er]. The magnitude of each shift then increases in [Y, Tm] and decreases in [Y, Yb]. The shift in the β proton on the center Pc is about 0.55 times that of the α proton. The ratio is almost constant over the six systems. The DFT calculation predicted the ratio with a sufficient accuracy (Table 2, "relative values").

The direction of paramagnetic shifts in the outer Pc is opposite to that of the center Pc and Pc*. The relative shifts are again almost constant over the six systems. The prediction by the DFT calculation is poor on these values. This is ascribed to the lack of polarization function in the DFT calculation.

Simulation of the SQUID and NMR Data. In the trivalent lanthanide ions under consideration (f^8−f^{13}), the total angular momentum J of the ground state takes the maximum value within the LS coupling scheme, that is, $J = L + S$. The simulations were carried out using the $2J + 1$ substates of the ground-state multiplet in each lanthanide system. The Hamiltonian of each system is written as

$$\hat{H} = \beta(\mathbf{L} + 2\mathbf{S})\cdot\mathbf{H} + \mathbf{F}$$

The first term of the right-hand side is Zeeman effect. The orbital and spin angular momentum matrices, **L** and **S**, are those represented in $\{|J,J_z\rangle\}$.

The second term is the LF potential, which can be expressed by the operator equivalent.[20] Following the notation by Abragam and Bleany,[21] the LF term belonging to C_4 point group is written as

$$\mathbf{F} = A_2^0\langle r^2\rangle\alpha\mathbf{O}_2^0 + A_4^0\langle r^4\rangle\beta\mathbf{O}_4^0 + A_4^4\langle r^4\rangle\beta\mathbf{O}_4^4 + A_6^0\langle r^6\rangle\gamma\mathbf{O}_6^0 + A_6^4\langle r^6\rangle\gamma\mathbf{O}_6^4 \quad (1)$$

The five coefficients $A_k^q\langle r^k\rangle$ are the parameters to be determined in the present fitting calculation. The $\mathbf{O}_k^q$ matrices are the polynomials of $\mathbf{J}^2$, $\mathbf{J}_z$, **J**, and $\mathbf{J}_+$, and their definitions are described in ref 21. The z axis is chosen to coincide the C_4 axis. The coefficients α, β, and γ are the constants tabulated by Stevens.[20]

With an arbitrary choice of a set of $A_k^q\langle r^k\rangle$ coefficients and a finite external field, the Hamiltonian gives a wave function and the magnetic moment for each substate. The magnetization of an ensemble at a certain temperature is obtained considering Maxwell−Boltzmann distribution. The magnetic moment per molecule was obtained by dividing the magnetization by the magnetic field applied. Its three principal values are denoted as χ_{xx}, χ_{yy}, and χ_{zz}, hereinafter.

The observed molar magnetic susceptibility, χ_m, of a powder sample is

$$\chi_m = N_A\bar{\chi}$$

$$\bar{\chi} = \frac{1}{3}(\chi_{xx} + \chi_{yy} + \chi_{zz})$$

where N_A is the Avogadro number. Because the paramagnetic center of each molecule is placed in a ligand field of C_4 symmetry, the following relation is held.

$$\chi_{xx} = \chi_{yy}$$

The dipolar contribution to the ^{1}H NMR paramagnetic shift is written as

$$\Delta\delta = \frac{\Delta\nu}{\nu} = \frac{(3\cos^3\theta - 1)}{2R^3}(\chi_{zz} - \bar{\chi})$$

where ν is the resonance frequency in the reference diamagnetic molecule, $\Delta\nu$ is the change in the frequency in the paramagnetic molecule, R is the distance between the paramagnetic center and the proton under consideration, and θ is the corresponding azimuth.[22] It should be noted that the magnetic moments appearing in the equation for ^{1}H NMR paramagnetic shift are the time-averaged values of one molecule and are therefore physically different entities from those observed in SQUID measurements. However, the ensemble-averaged value and the time-averaged value actually coincide in the present case.

Fitting the calculation to the experimental values was carried out with the simplex algorithm.[23] The test function to be minimized was the sum of two values, the error from the experimental values in $\chi_m T$ and that in $\Delta\delta$. The former is the root-mean-square deviation from the observed $\chi_m T$ values at 42 sampling points, which are 2, 4, 8, 15, 30, 70, and 150 K in the six lanthanide systems. The latter is the root-mean-square deviation from the six $\Delta\delta$ values of the α proton on the center Pc.

It is expected that the LF parameters vary fairly regularly from the f^8 system to the f^{13} system. We have employed an assumption that each parameter is expressed as a linear function of the number of f electrons, n:

$$A_k^q\langle r^k\rangle(n) = a_k^q + b_k^q(n - 10) \qquad n = 8, 9, ..., 13$$

The actual calculations were performed in two stages. In the first stage, b_k^q were fixed to zero. From a set of guess parameters for a_k^q, the local minimum for the test function was explored by five-dimensional simplex minimization. After repeating performances of this step with different initial guesses, a few candidate sets of a_k^q were selected. The second stage used these sets as initial guesses. Through ten-dimensional simplex minimization calculations, which moves both a_k^q and b_k^q, we obtained fully optimized LF parameter sets, from which the best set has been chosen.

Table 3 lists thus obtained LF parameters of the six lanthanide systems. Figure 4 shows the theoretical $\chi_m T$ vs T plot using the

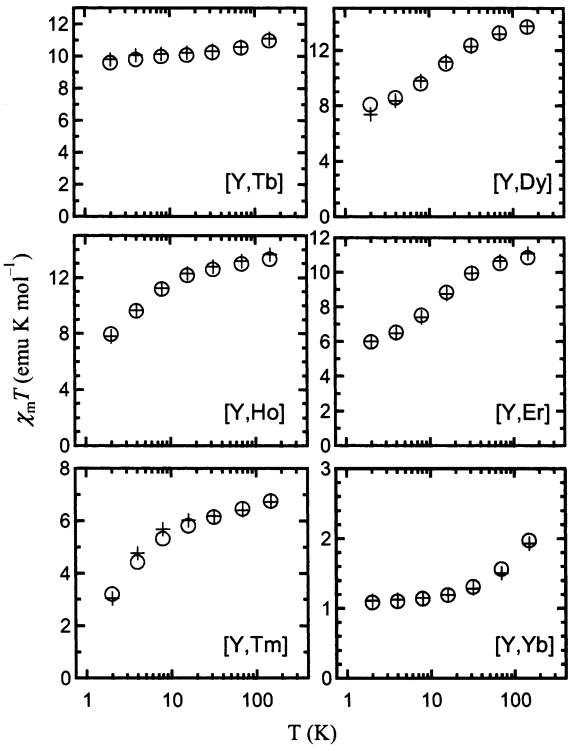

Figure 4. Theoretical temperature dependence of the $\chi_m T$ values (crosses) and the experimental data used for fitting (circles).

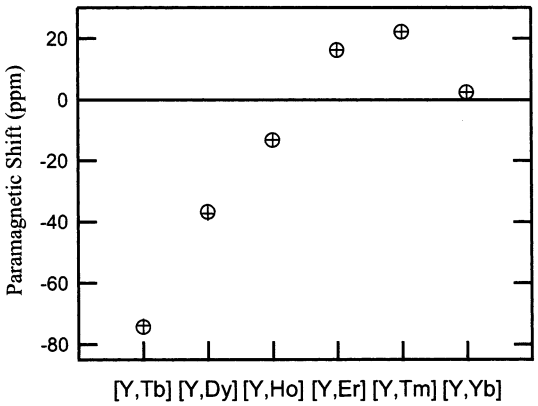

Figure 5. Theoretical (crosses) and observed (circles) paramagnetic shifts of the NMR signal of the α-proton on the central Pc ligands in [Y, Ln] (Ln = Tb, Dy, Ho, Er, Tm, and Yb).

TABLE 3: Determined LF Parameters (in cm^{-1}) for PcYPcLnPc(OC$_4$H$_9$)$_8$

Ln	$A_2^0\langle r^2\rangle$	$A_4^0\langle r^4\rangle$	$A_4^4\langle r^4\rangle$	$A_6^0\langle r^6\rangle$	$A_6^4\langle r^6\rangle$
Tb	293	−197	863	15.1	357
Dy	268	−190	828	15.1	327
Ho	244	−183	792	15.0	296
Er	220	−176	757	15.0	265
Tm	195	−169	721	14.9	235
Yb	171	−162	686	14.8	204

parameters. These parameters well reproduced the experimental $\chi_m T$ curve. Figure 5 shows the comparison of the theoretical and experimental $\Delta\delta$ values. It is seen that the obtained parameters reproduced both the SQUID and ^{1}H NMR data with a good accuracy.

Arnold et al. reported synthesis of a series of homo-dinuclear lanthanide Pc complexes and discussed the origin of the paramagnetic shifts in ^{1}H NMR spectrum.[15] They concluded that the paramagnetic shifts contain significant contributions

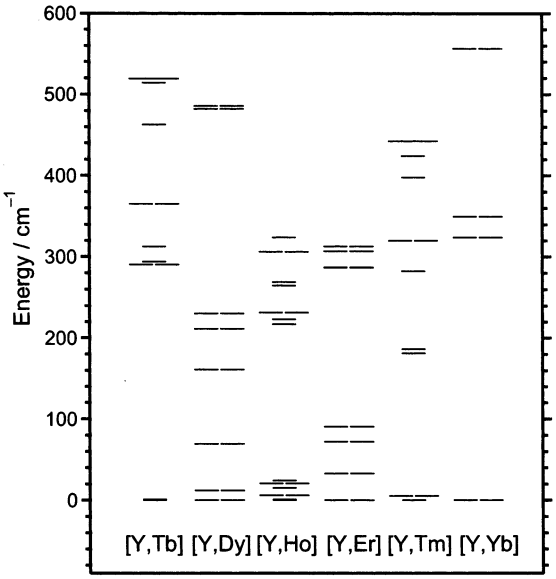

Figure 6. Energy diagram for the ground-state multiplets of [Y, Ln] (Ln = Tb, Dy, Ho, Er, Tm, and Yb).

from Fermi contact term,[15] which is usually expected to be very small unless the nucleus under consideration is immediately adjacent to the lanthanide ion.[22] Their arguments, however, had a serious weakness in the spin expectation value, $\langle S_z\rangle$, and a magnetic constant D used in the analysis. The values employed were those determined for lanthanide ions doped in a $LaCl_3$ matrix,[24,25] which gives a C_{3h} ligand field and therefore a different LF term expression (eq 3 in ref 25) from that of the Pc triple-deckers, eq 1. Our analysis, which assumes only the dipolar contribution, clearly shows that neglect of the Fermi contact term is appropriate, at least in the [Y, Ln] series. We are currently investigating the homo-dinuclear cases with the method described here. The result will be reported in a subsequent paper.

Electronic Structures of the [Y, Ln] Complexes. With the parameters obtained above, the electronic structures of the ground states of the six lanthanide systems are determined. Figure 6 shows the energy levels of the $2J + 1$ sublevels of the ground state of each system.

(1) [Y, Tb] System. The lowest two substates are assigned to $\{|6\rangle + |-6\rangle\}$ and $\{|6\rangle - |-6\rangle\}$, the components of which have the largest $|J_z|$ value within the ground-state manifold (Table 4). The next sublevel lies about 300 cm^{-1} above them. This large splitting gives predominant occupation on the lowest two levels. The dominancy is kept up to relatively high temperature (99.5% at 70 K). The magnetic behavior of this molecule at under 70 K is essentially described by the $|6\rangle$ and $|-6\rangle$ substates.

(2) [Y, Dy] System. The lowest substate is degenerate and assigned to $|11/2\rangle$ and $|-11/2\rangle$ (Table 5). The next substate, characterized by $|13/2\rangle$ and $|-13/2\rangle$ is 12 cm^{-1} above the lowest level. At 2 K, the population of the $|\pm 11/2\rangle$ state is 99.98%. The population drops to 54% at 50 K, while that of the $|\pm 13/2\rangle$ level gains 38%. The relatively rapid change in $\chi_m T$ in the low-temperature range is ascribed to the rapid increase of the population to the $|\pm 13/2\rangle$ level.

(3) [Y, Ho] System. This system greatly differs in substate level distribution from the other systems. The lowest six substates are located within 25 cm^{-1} (Table 6). At 2 K, the sum of the populations in two lowest substates $\{|6\rangle - |-6\rangle\}$ and $\{|6\rangle + |-6\rangle\}$ is 98.2% and the next degenerate lowest state $\{|5\rangle \pm |-5\rangle\}$ is populated by 1.8%. The latter value quickly rises to 15% at 5 K. At 50 K, the population on the sixth lowest

TABLE 4: Energies and Wave Functions of the Ground-State Multiplets of [Y, Tb]

energy (cm^{-1})	wave functions[a]					
0	$0.70\|6\rangle$	$-0.70\|-6\rangle$	$+0.03\|2\rangle$	$-0.03\|-2\rangle$		
0.2	$0.70\|6\rangle$	$+0.70\|-6\rangle$				
291	$0.53\|1\rangle$	$+0.53\|-1\rangle$	$-0.36\|5\rangle$	$-0.36\|-5\rangle$	$-0.28\|3\rangle$	$-0.28\|-3\rangle$
291	$0.53\|1\rangle$	$-0.53\|-1\rangle$	$-0.36\|5\rangle$	$+0.36\|-5\rangle$	$+0.28\|3\rangle$	$-0.28\|-3\rangle$
294	$0.86\|0\rangle$	$-0.35\|4\rangle$	$-0.35\|-4\rangle$			
312	$0.70\|2\rangle$	$-0.70\|-2\rangle$	$+0.03\|6\rangle$	$-0.03\|-6\rangle$		
365	$0.59\|5\rangle$	$+0.59\|-5\rangle$	$-0.26\|3\rangle$	$-0.26\|-3\rangle$	$+0.26\|1\rangle$	$+0.26\|-1\rangle$
365	$0.59\|5\rangle$	$-0.59\|-5\rangle$	$+0.26\|3\rangle$	$-0.26\|-3\rangle$	$+0.26\|1\rangle$	$-0.26\|-1\rangle$
463	$0.70\|4\rangle$	$-0.70\|-4\rangle$				
514	$0.70\|2\rangle$	$+0.70\|-2\rangle$				
519	$0.58\|3\rangle$	$+0.58\|-3\rangle$	$+0.38\|1\rangle$	$+0.38\|-1\rangle$	$+0.08\|5\rangle$	$+0.08\|-5\rangle$
519	$0.58\|3\rangle$	$-0.58\|-3\rangle$	$-0.38\|1\rangle$	$+0.38\|-1\rangle$	$-0.08\|5\rangle$	$+0.08\|-5\rangle$
519	$0.61\|4\rangle$	$+0.61\|-4\rangle$	$+0.50\|0\rangle$			

[a] Terms with a coefficient greater than 0.02 are shown. The coefficients have been rounded down to the nearest hundredth.

TABLE 5: Energies and Wave Functions of the Ground-State Multiplets of [Y, Dy]

energy (cm^{-1})	wave functions						
0	$0.99\|11/2\rangle$	$+0.08\|3/2\rangle$	$+0.03\|-5/2\rangle$				
0	$0.99\|-11/2\rangle$	$+0.08\|-3/2\rangle$	$+0.03\|5/2\rangle$				
12	$0.99\|-13/2\rangle$	$-0.02\|-5/2\rangle$					
12	$0.99\|13/2\rangle$	$-0.02\|5/2\rangle$					
69	$0.81\|9/2\rangle$	$+0.47\|-9/2\rangle$	$+0.21\|1/2\rangle$	$+0.18\|-7/2\rangle$	$+0.12\|-1/2\rangle$	$+0.10\|7/2\rangle$	
69	$0.81\|-9/2\rangle$	$-0.47\|9/2\rangle$	$+0.21\|-1/2\rangle$	$+0.18\|7/2\rangle$	$-0.13\|1/2\rangle$	$-0.10\|-7/2\rangle$	
161	$0.87\|7/2\rangle$	$-0.28\|-9/2\rangle$	$+0.28\|-1/2\rangle$	$-0.26\|15/2\rangle$	$-0.07\|-7/2\rangle$	$+0.02\|9/2\rangle$	$-0.02\|1/2\rangle$
161	$0.87\|-7/2\rangle$	$-0.28\|9/2\rangle$	$+0.28\|1/2\rangle$	$-0.26\|-15/2\rangle$	$+0.07\|7/2\rangle$	$-0.02\|-9/2\rangle$	$+0.02\|-1/2\rangle$
211	$0.78\|5/2\rangle$	$+0.57\|-3/2\rangle$	$+0.17\|-5/2\rangle$	$+0.13\|3/2\rangle$	$-0.07\|-11/2\rangle$	$+0.02\|11/2\rangle$	
211	$0.78\|-5/2\rangle$	$+0.57\|3/2\rangle$	$-0.17\|5/2\rangle$	$-0.13\|-3/2\rangle$	$-0.07\|11/2\rangle$	$+0.02\|-11/2\rangle$	
230	$0.95\|-15/2\rangle$	$+0.23\|-7/2\rangle$	$+0.11\|1/2\rangle$	$-0.10\|15/2\rangle$	$-0.05\|9/2\rangle$		
230	$0.95\|15/2\rangle$	$+0.23\|7/2\rangle$	$+0.11\|-1/2\rangle$	$+0.10\|-15/2\rangle$	$-0.05\|-9/2\rangle$		
482	$0.84\|-1/2\rangle$	$+0.35\|1/2\rangle$	$-0.33\|7/2\rangle$	$-0.15\|-9/2\rangle$	$-0.14\|-7/2\rangle$	$-0.06\|9/2\rangle$	$-0.02\|15/2\rangle$
482	$0.84\|1/2\rangle$	$-0.35\|-1/2\rangle$	$-0.33\|-7/2\rangle$	$-0.15\|9/2\rangle$	$+0.14\|7/2\rangle$	$+0.06\|-9/2\rangle$	$-0.02\|-15/2\rangle$
486	$0.76\|-3/2\rangle$	$-0.56\|5/2\rangle$	$-0.25\|3/2\rangle$	$+0.18\|-5/2\rangle$	$-0.04\|-11/2\rangle$		
486	$0.76\|3/2\rangle$	$-0.56\|-5/2\rangle$	$+0.25\|-3/2\rangle$	$-0.18\|5/2\rangle$	$-0.04\|11/2\rangle$		

TABLE 6: Energies and Wave Functions of the Ground-State Multiplets of [Y, Ho]

energy (cm^{-1})	wave functions							
0	$0.64\|6\rangle$	$+0.64\|-6\rangle$	$+0.29\|2\rangle$	$+0.29\|-2\rangle$				
1	$0.64\|6\rangle$	$-0.64\|-6\rangle$	$+0.29\|2\rangle$	$-0.29\|-2\rangle$				
6	$0.67\|5\rangle$	$+0.67\|-5\rangle$	$+0.18\|1\rangle$	$+0.18\|-1\rangle$	$+0.07\|3\rangle$	$+0.07\|-3\rangle$	$+0.07\|7\rangle$	$+0.07\|-7\rangle$
6	$0.67\|5\rangle$	$-0.67\|-5\rangle$	$+0.18\|1\rangle$	$-0.18\|-1\rangle$	$-0.07\|3\rangle$	$+0.07\|-3\rangle$	$-0.07\|7\rangle$	$+0.07\|-7\rangle$
15	$0.63\|4\rangle$	$+0.63\|-4\rangle$	$+0.29\|8\rangle$	$+0.29\|-8\rangle$	$+0.17\|0\rangle$			
21	$0.51\|7\rangle$	$+0.51\|-7\rangle$	$+0.46\|3\rangle$	$+0.46\|-3\rangle$	$-0.11\|5\rangle$	$-0.11\|-5\rangle$		
21	$0.51\|7\rangle$	$-0.51\|-7\rangle$	$+0.46\|3\rangle$	$-0.46\|-3\rangle$	$+0.11\|5\rangle$	$-0.11\|-5\rangle$		
24	$0.63\|4\rangle$	$-0.63\|-4\rangle$	$+0.30\|8\rangle$	$-0.30\|-8\rangle$				
217	$0.63\|8\rangle$	$+0.63\|-8\rangle$	$-0.26\|4\rangle$	$-0.26\|-4\rangle$	$-0.22\|0\rangle$			
223	$0.63\|8\rangle$	$-0.63\|-8\rangle$	$-0.30\|4\rangle$	$+0.30\|-4\rangle$				
232	$0.51\|3\rangle$	$+0.51\|-3\rangle$	$-0.47\|7\rangle$	$-0.47\|-7\rangle$	$+0.08\|1\rangle$	$+0.08\|-1\rangle$	$-0.03\|5\rangle$	$-0.03\|-5\rangle$
235	$0.51\|3\rangle$	$-0.51\|-3\rangle$	$-0.47\|7\rangle$	$+0.47\|-7\rangle$	$-0.08\|1\rangle$	$+0.08\|-1\rangle$	$+0.03\|5\rangle$	$-0.03\|-5\rangle$
265	$0.64\|2\rangle$	$+0.64\|-2\rangle$	$-0.29\|6\rangle$	$-0.29\|-6\rangle$				
269	$0.64\|2\rangle$	$-0.64\|-2\rangle$	$-0.29\|6\rangle$	$+0.29\|-6\rangle$				
306	$0.67\|1\rangle$	$-0.67\|-1\rangle$	$-0.17\|5\rangle$	$+0.17\|-5\rangle$	$+0.07\|3\rangle$	$-0.07\|-3\rangle$	$-0.04\|7\rangle$	$+0.04\|-7\rangle$
307	$0.67\|1\rangle$	$+0.67\|-1\rangle$	$-0.17\|5\rangle$	$-0.17\|-5\rangle$	$-0.07\|3\rangle$	$-0.07\|-3\rangle$	$+0.04\|7\rangle$	$+0.04\|-7\rangle$
323	$0.95\|0\rangle$	$-0.17\|4\rangle$	$-0.17\|-4\rangle$	$+0.10\|8\rangle$	$+0.10\|-8\rangle$			

state at 24 cm^{-1} reaches 8.4%. All of these six substates are needed to describe the magnetic behavior of the [Y, Ho] system in the low-temperature range.

(4) [Y, Er] System. The lowest substate is a degenerate pair of $|1/2\rangle$ and $|-1/2\rangle$ (Table 7). The magnetic behavior is predominantly described by the $|\pm 1/2\rangle$ states at 2 K. The contribution from the second lowest state, $|\pm 3/2\rangle$, becomes nonnegligible at about 10 K, as the population of the state increases to 0.8%.

(5) [Y, Tm] System. In this system, three substates, that is, the nondegenerate $\{|2\rangle - |-2\rangle\}$, the degenerate pair $\{|1\rangle \pm |-1\rangle\}$, and $|0\rangle$, lie within 8 cm^{-1} (Table 8). At 2 K, the population distribution is 94.7% in $\{|2\rangle - |-2\rangle\}$, 5.0% in $\{|1\rangle \pm |-1\rangle\}$, and 0.3% in $|0\rangle$. These ratios change to 44%, 42%, and 14% at 10 K, respectively. Because the fourth substate lies at fairly high energy (about 180 cm^{-1}), the magnetic behavior of this system in the low-temperature range is determined by the three lowest substates.

(6) [Y, Yb] System. The main component of the degenerate lowest substate is $|\pm 5/2\rangle$ (Table 9). In addition, the $|\pm 3/2\rangle$ state has considerably large contribution (28%), which has not been seen in the other systems. Because of the mixing, the magnetic behavior of the system cannot be approximated by those of pure $|j_z\rangle$ states. There is a large energy gap between the lowest and the second substates. The population in the lowest substate stays more than 99% up to 90 K, meaning that the magnetic behavior below the temperature is determined solely by the lowest pair.

Conclusions

We have obtained the LF parameters for the paramagnetic lanthanide ions in the dinuclear Pc triple-decker complexes

TABLE 7: Energies and Wave Functions of the Ground-State Multiplets of [Y, Er]

energy (cm^{-1})	wave functions					
0	$0.96\|1/2\rangle$	$-0.20\|9/2\rangle$	$-0.14\|-7/2\rangle$	$+0.08\|-15/2\rangle$		
0	$0.96\|-1/2\rangle$	$-0.20\|-9/2\rangle$	$-0.14\|7/2\rangle$	$+0.08\|15/2\rangle$		
33	$0.92\|3/2\rangle$	$-0.35\|11/2\rangle$	$-0.10\|-5/2\rangle$	$+0.06\|-13/2\rangle$		
33	$0.92\|-3/2\rangle$	$-0.35\|-11/2\rangle$	$-0.10\|5/2\rangle$	$+0.06\|13/2\rangle$		
72	$0.65\|5/2\rangle$	$-0.53\|13/2\rangle$	$-0.39\|-5/2\rangle$	$+0.32\|-13/2\rangle$	$+0.09\|-3/2\rangle$	$-0.04\|-11/2\rangle$
72	$0.65\|-5/2\rangle$	$-0.53\|-13/2\rangle$	$+0.39\|5/2\rangle$	$-0.32\|13/2\rangle$	$+0.09\|3/2\rangle$	$-0.04\|11/2\rangle$
91	$0.88\|-15/2\rangle$	$-0.44\|-7/2\rangle$	$-0.13\|1/2\rangle$	$+0.04\|9/2\rangle$	$+0.02\|15/2\rangle$	
91	$0.88\|15/2\rangle$	$-0.44\|7/2\rangle$	$-0.13\|-1/2\rangle$	$+0.04\|-9/2\rangle$	$-0.02\|-15/2\rangle$	
287	$0.75\|-13/2\rangle$	$+0.61\|-5/2\rangle$	$+0.16\|13/2\rangle$	$+0.13\|5/2\rangle$	$-0.05\|11/2\rangle$	
287	$0.75\|13/2\rangle$	$+0.61\|5/2\rangle$	$-0.16\|-13/2\rangle$	$-0.13\|-5/2\rangle$	$-0.05\|-11/2\rangle$	
287	$0.84\|-7/2\rangle$	$+0.44\|-15/2\rangle$	$-0.29\|7/2\rangle$	$+0.02\|1/2\rangle$		
287	$0.84\|7/2\rangle$	$+0.44\|15/2\rangle$	$-0.29\|-7/2\rangle$	$+0.02\|-1/2\rangle$		
307	$0.90\|-9/2\rangle$	$+0.24\|7/2\rangle$	$+0.23\|9/2\rangle$	$+0.11\|15/2\rangle$	$+0.06\|-7/2\rangle$	
307	$0.90\|9/2\rangle$	$+0.24\|-7/2\rangle$	$-0.23\|-9/2\rangle$	$+0.11\|-15/2\rangle$	$-0.06\|7/2\rangle$	
313	$0.92\|-11/2\rangle$	$+0.36\|-3/2\rangle$	$+0.06\|11/2\rangle$	$+0.04\|5/2\rangle$	$+0.04\|13/2\rangle$	
313	$0.92\|11/2\rangle$	$+0.36\|3/2\rangle$	$-0.06\|-11/2\rangle$	$+0.04\|-5/2\rangle$	$+0.04\|-13/2\rangle$	

TABLE 8: Energies and Wave Functions of the Ground-State Multiplets of [Y, Tm]

energy (cm^{-1})	wave functions					
0	$0.70\|2\rangle$	$-0.70\|-2\rangle$	$+0.06\|6\rangle$	$-0.06\|-6\rangle$		
5	$0.64\|1\rangle$	$+0.64\|-1\rangle$	$-0.29\|3\rangle$	$-0.29\|-3\rangle$	$-0.02\|5\rangle$	$-0.02\|-5\rangle$
5	$0.64\|1\rangle$	$-0.64\|-1\rangle$	$+0.29\|3\rangle$	$-0.29\|-3\rangle$	$-0.02\|5\rangle$	$+0.02\|-5\rangle$
8	$0.96\|0\rangle$	$-0.17\|4\rangle$	$-0.17\|-4\rangle$			
181	$0.69\|6\rangle$	$+0.69\|-6\rangle$	$+0.12\|2\rangle$	$+0.12\|-2\rangle$		
186	$0.70\|6\rangle$	$-0.70\|-6\rangle$	$-0.06\|2\rangle$	$+0.06\|-2\rangle$		
282	$0.69\|2\rangle$	$+0.69\|-2\rangle$	$-0.12\|6\rangle$	$-0.12\|-6\rangle$		
319	$0.64\|3\rangle$	$+0.64\|-3\rangle$	$+0.29\|1\rangle$	$+0.29\|-1\rangle$	$-0.04\|5\rangle$	$-0.04\|-5\rangle$
319	$0.64\|3\rangle$	$-0.64\|-3\rangle$	$-0.29\|1\rangle$	$+0.29\|-1\rangle$	$+0.04\|5\rangle$	$-0.04\|-5\rangle$
398	$0.70\|4\rangle$	$-0.70\|-4\rangle$				
425	$0.68\|4\rangle$	$+0.68\|-4\rangle$	$+0.25\|0\rangle$			
442	$0.70\|5\rangle$	$-0.70\|-5\rangle$	$+0.04\|1\rangle$	$-0.04\|-1\rangle$	$-0.02\|3\rangle$	$+0.02\|-3\rangle$
442	$0.70\|5\rangle$	$+0.70\|-5\rangle$	$+0.04\|1\rangle$	$+0.04\|-1\rangle$	$+0.02\|3\rangle$	$+0.02\|-3\rangle$

TABLE 9: Energies and Wave Functions of the Ground-State Multiplets of [Y, Yb]

energy (cm^{-1})	wave functions	
0	$0.84\|5/2\rangle$	$+0.52\|-3/2\rangle$
0	$0.84\|-5/2\rangle$	$+0.52\|3/2\rangle$
323	$0.84\|-3/2\rangle$	$-0.52\|5/2\rangle$
323	$0.84\|3/2\rangle$	$-0.52\|-5/2\rangle$
349	$0.96\|-1/2\rangle$	$+0.26\|7/2\rangle$
349	$0.96\|1/2\rangle$	$+0.26\|-7/2\rangle$
556	$0.96\|-7/2\rangle$	$-0.26\|1/2\rangle$
556	$0.96\|7/2\rangle$	$-0.26\|-1/2\rangle$

through a synthesis of the series of new lanthanide hetero-dinuclear complexes and theoretical analysis of the SQUID and ^{1}H NMR data. The simultaneous use of the SQUID data and ^{1}H NMR data for the six lanthanide systems under the assumption that each LF parameter is a linear function of the number of f electrons has led to a successful convergence of the LF parameters, $A_k^q\langle r^k\rangle$. The obtained $A_k^q\langle r^k\rangle$ well reproduces the temperature dependence of magnetic susceptibility and paramagnetic shift of ^{1}H NMR signals. The sublevel structures of the ground states of the six lanthanide complexes have been elucidated. The information presented in this work shall provide a firm foundation for further studies on the systems having multiple paramagnetic lanthanide centers.

Acknowledgment. This work was partially supported by a Grant-in-Aid for Science Research No. 13740375 from the Ministry of Education, Science, Sports and Culture in Japan. The authors express their gratitude to Prof. Toshiaki Enoki, Dr. Hirohiko Sato, Dr. Akira Miyazaki, and Dr. Kazuyuki Takai in Tokyo Institute of Technology for the permission to use the SQUID instrument and invaluable help. Also thanks are due to Prof. Katsumi Kakinuma and Prof. Tadashi Eguchi for the permission to use the NMR spectrometer. Last, but not least, we gratefully thank Dr. Ken Ohmori for the invaluable help on the NMR measurements.

References and Notes

(1) M′Sadak, M.; Roncali, J.; Garnir, F. *J. Chim. Phys.* **1986**, *83*, 211.
(2) Kasuga, K.; Ando, M.; Morimoto, H.; Isa, M. *Chem. Lett.* **1986** 1095.
(3) Buchler, J. W.; De Cian, A.; Fischer, J.; Kihn-Botulinski, M.; Paulus, H.; Weiss, R. *J. Am. Chem. Soc.* **1986**, *108*, 3652.
(4) Chabach, D.; Lachkar, M.; De Cian, A.; Fischer, J.; Weiss, R. *New J. Chem.* **1992**, *16*, 431.
(5) Abbreviations used: OEP = 2,3,7,8,12,13,17,18-octaethylporphyrin dianion; Pc = phthalocyanine dianion; TPP = *meso*-tetra(phenyl)porphyrin dianion; T(*p*-MeOP)P = *meso*-tetra(anisyl)porphyrin dianion; $Pc(OMe)_8$ = 2,3,9,10,16,17,23,24-octa-methoxy(phthalocyanine) dianion.
(6) Ishikawa, N.; Kaizu, Y. *J. Phys. Chem.* **1996**, *100*, 8722.
(7) Ishikawa, N.; Kaizu, Y. *Chem. Phys. Lett.* **1994**, *228*, 625.
(8) Ishikawa, N.; Ohno, O.; Kaizu, Y.; Kobayashi, H. *J. Phys. Chem.* **1992**, *96*, 8832.
(9) Ishikawa, N.; Kaizu, Y. *J. Porphyrins and Phthalocyanines* **1999**, *3*, 514.
(10) Ishikawa, N.; Kaizu, Y. *Chem. Phys. Lett.* **1995**, *236*, 50.
(11) Ishikawa, N.; Okubo, T.; Kaizu, Y. *Inorg. Chem.* **1999**, *38*, 3173.
(12) Gross, T.; Chevalier, F.; Lindsey, J. S. *Inorg. Chem.* **2001**, *40*, 4762.
(13) Abbreviations used: tBPc = tetra-*tert*-butylphthalocyanine dianion; TTP = *meso*-tetra(*p*-tolyl)porphyrin dianion.
(14) Liu, W.; Jiang, J.; Pan, N.; Arnold, D. P. *Inorg. Chim. Acta* **2000**, *310*, 140.
(15) Arnold, D. P.; Jiang, J. *J. Phys. Chem. A* **2001**, *105*, 7533.
(16) Becke, A. D. *J. Chem. Phys.* **1993**, *98*, 5648−5652.
(17) Frisch, M. J.; Trucks, G. W.; Schlegel, H. B.; Scuseria, G. E.; Robb, M. A.; Cheeseman, J. R.; Zakrzewski, V. G.; Montgomery, J. A., Jr.; Stratmann, R. E.; Burant, J. C.; Dapprich, S.; Millam, J. M.; Daniels, A. D.; Kudin, K. N.; Strain, M. C.; Farkas, O.; Tomasi, J.; Barone, V.; Cossi, M.; Cammi, R.; Mennucci, B.; Pomelli, C.; Adamo, C.; Clifford, S.; Ochterski, J.; Petersson, G. A.; Ayala, P. Y.; Cui, Q.; Morokuma, K.; Malick, D. K.; Rabuck, A. D.; Raghavachari, K.; Foresman, J. B.; Cioslowski, J.; Ortiz, J. V.; Stefanov, B. B.; Liu, G.; Liashenko, A.; Piskorz, P.; Komaromi, I.; Gomperts, R.; Martin, R. L.; Fox, D. J.; Keith, T.; Al-Laham, M. A.; Peng, C. Y.; Nanayakkara, A.; Gonzalez, C.; Challacombe, M.; Gill, P. M. W.; Johnson, B. G.; Chen, W.; Wong, M. W.; Andres, J. L.; Head-Gordon,

M.; Replogle, E. S.; Pople, J. A. *Gaussian 98*, revision A.11; Gaussian, Inc.: Pittsburgh, PA, 1998.

(18) (a) Hay, P. J.; Wadt, W. R. *J. Chem. Phys.* **1985**, *82*, 270. (b) Hay, P. J.; Wadt, W. R. *J. Chem. Phys.* **1985**, *82*, 284. (c) Hay, P. J.; Wadt, W. R. *J. Chem. Phys.* **1985**, *82*, 299.

(19) Dunning, T. H., Jr.; Hay, P. J. In *Modern Theoretical Chemistry*; Schaefer, H. F., III., Ed.; Plenum: New York, 1976; pp 1−28.

(20) Stevens, K. W. H. *Proc. Phys. Soc. A* **1952**, *65*, 209.

(21) Abragam, A.; Bleany, B. *Electron Paramagnetic Resonance*; Clarendon Press: Oxford, U.K., 1970.

(22) Bleany, B. *J. Magn. Reson.* **1972**, *8*, 91.

(23) Nelder, J. A.; Mead, R. *Comput. J.* **1965**, *7*, 308.

(24) Golding, R. M.; Halton, M. P. *Aust. J. Chem.* **1972**, *25*, 2577.

(25) Golding, R. M.; Pyykkö, P. *Mol. Phys.* **1973**, *26*, 1389.